[REVISION 2]

Pyrite stability and chalcophile element mobility in a hot Eocene forearc of the Pacific Rim Terrane, Vancouver Island, Canada

Alexander C. Geen and Dante Canil*

School of Earth and Ocean Science, University of Victoria, Victoria, Canada V8W 3P6

*corresponding author dcanil@uvic.ca

Keywords: sulfide, chalcophile, metamorphism, forearc, phase equilibria, gold

Words total = 8553

Abstract

The conditions of pyrite (Py) stability inform the extent of S mobility during prograde metamorphism, the formation of orogenic Au deposits and the S cycle in subduction zones. The variables that affect Py stability and chalcophile element mobility are investigated in the Pacific Rim Terrane of Vancouver Island, Canada, where sulfide-bearing carbonaceous sediments have been metamorphosed from 230 to 600 °C and 4 kbar by mid-ocean ridge subduction in a hot fore arc setting during the Eocene. The petrographic evidence in the rocks shows Py can co-exist with pyrrhotite (Po) over a wide temperature window to > 550 °C as preserved in porphyroblasts of andulasite, staurolite and garnet. Conversely, equilibrium phase diagrams constructed for the rock compositions conflict with observations and suggest the breakdown of primary Py occurs over a narrow temperature range below 400 °C. The phase diagrams are consistent with the

coexistence of Py and Po up to lower amphibolite facies only if S locally comprises a much greater proportion involved in a reaction than that of the overall bulk rock composition used in the calculations. While the chemistry of the bulk rocks and Po included in porphyroblasts show mobilization of H_2O and S with increasing metamorphic grade of the forearc, this process appears unrelated to the distribution of chalcophile elements or Au deposits found in the Pacific Rim Terrane.

Introduction

Sulfur is a minor component of the Earth's crust, but has a wide range of oxidation states (2- to 6+) and affinity for chalcophile elements, making its behaviour of significant interest in metamorphic systems and ore deposits. In marine siliciclastic sediments, S is typically bound in sulfides derived from biogenic, diagenetic, and hydrothermal processes (Goldhaber 2003). Among carbonaceous marine sediments, pyrite (Py) is the most abundant sulfide and may occur as disseminated anhedral grains, laminae and bands, framboids, spherulites, and cubic euhedra (Goldhaber 2003). Because sedimentary and diagenetic Py are commonly enriched in Zn, Cu, Mo, Pb, Au and Ag (Thomas et al. 2011; Large et al. 2012), the stability of Py during prograde metamorphism bears on their mobility of these economically important elements (Pitcairn et al. 2006, 2010, 2015).

Sulfide stability also bears on the global S cycle. The S subducted into the mantle in oceanic lithosphere becomes a potentially important redox agent in the mantle contingent upon the P-T stability fields of sulfide and sulfate, and the P-T paths taken by subducted slabs (Mungall 2002; Evans,2012; Canil and Fellows 2017; Walters et al. 2020). The behavior of sulfides in the shallow forearc of the subduction zone is significant for S mobility and ore

genesis (Pitcairn et al. 2010). During low pressure prograde metamorphism of carbonaceous sediments, one reaction involving sulfide can be (Tomkins 2010):

$$FeS_2 = FeS + 0.5S_2 \quad [1]$$

where for every mol of Py consumed, one mole each of pyrrhotite (Po) and S is produced. A devolatilizing carbonaceous metapelite could also drive the production of reduced S compounds, such as in the reaction (Ferry 1981):

$$2FeS_2 + 2H_2O\,(fluid) + C(Gr) = 2FeS + 2H_2S_{\,(fluid)} + CO_{2\,(fluid)} \quad [2]$$

In this manner, S could be mobilized in a metamorphic fluid and liberated from the rock (Tomkins 2010) or available to react with other minerals. Either way, the breakdown of Py enables the redistribution of trace elements previously hosted therein (Large et al. 2012). There is significant variability in the degree of mobilization of base metals such as Cu, As, Zn, and Pb (Hammerli et al. 2016; Stepanov 2021), and a growing body of evidence suggests liberated Au is efficiently transported as HS- ligands at low temperatures in metamorphic fluids (Pokrovski et al. 2009). Therefore, delineating the conditions of S mobility is central for understanding mechanisms of chalcophile element and Au distribution during prograde metamorphism. The development of internally consistent thermodynamic data for common sulfides like Py and Po (Evans et al. 2010) has advanced models of sulfide-silicate phase relations, but has produced contrasting results. When reactions between sulfides and iron-bearing silicates are precluded, the models show Py stability can persist until conditions approximating terminal chlorite breakdown, with concomitant fluid production (Tomkins, 2010). Conversely, some models of sulfide-silicate phase relations suggest that the Py-Po transition is instead a narrow, low-temperature threshold that is influenced by bulk rock chemistry (Zhong et al. 2015).

Sulfide phase relations vary with pressure, temperature and protolith composition (P-T-X), necessitating careful consideration of both protolith and the P-T evolution of rocks. This study seeks to test these variables by examining sulfide stability and chalcophile element changes from sub-greenschist to amphibolite facies in the Pacific Rim Terrane on southern Vancouver Island, Canada, where sulfide-bearing carbonaceous forearc metasediments have been metamorphosed from 230 to 600 °C at a broadly low pressure of 4 kbar (Seyler et al 2022; Geen and Canil 2023). Gold deposits in greenschist-amphibolite grade rocks in the terrane have been the subject of periodic economic interest (Houle, 2011). Thus, the Pacific Rim Terrane is complementray to evaluate controls on prograde loss of S, and its potential consequences for forming an orogenic Au deposit in a forearc setting. The occurrence of Py, Po, sulfide, and whole rock chemistry in the terrane are compared with representative phase diagrams of the rocks to examine controls on sulfide stability in the natural metamorphic rock record and assess any role of S re-distribution in metal concentration.

Regional Geology and Metamorphism

The Pacific Rim Terrane is a package of metasedimentary and subsidiary metaigneous rocks accreted to Wrangellia, two of the three westernmost terranes that make up the western North American Cordillera (Fig. 1). Metamorphism up to amphibolite facies coincided with isoclinal folding that transposed depositional fabrics into parallelism, obscured regional stratigraphy, followed by top-to-east shear and large-scale open folding (Fairchild and Cowan 1982; Groome et al, 2003; Jakob et al. 2016). The terrane comprises three sub-units, two of which are considered in this study: the Leech River Complex and Pandora Peak Unit (Fig. 1).

The Leech River Complex has a depositional age as young as 61 Ma (Geen 2021; Seyler et al. 2022) and comprises mostly interfoliated carbonaceous argillites, schists, arkoses and

88 greywackes, and quartz-rich paragneisses with psammitic and pelitic bulk compositions.
89 Subsidiary but common meter to decimeter scale layers of metabasic rocks are intercalated with
90 the metasedimentary rocks at all grades. Within the Leech River Complex, volumetrically minor
91 tonalite sills with crystallization ages of 51 to 48 Ma (Groome et al. 2003; Seyler et al. 2022) are
92 also interfoliated with the metasedimentary rocks but lack any contact aureoles.

93 To the north, the Pandora Peak Unit comprises clastic argillites, tectonites, radiolarian-
94 bearing ribbon metacherts, metabasalts, and meta-ultramafic olistostromes. Metamorphic
95 assemblages of lawsonite and glaucophane suggest sub-to-low blueschist facies conditions for
96 this unit. Metamorphic temperature constrained by geothermometry increases southward from
97 230 °C to 600 °C across the Pacific Rim Terrane (Fig 1). The metamorphic gradient is
98 interpreted to have resulted from subcretion a hot, young nascent oceanic ridge or plateau at ~ 52
99 Ma, represented by the Crescent-Siletzia Terrane to the south (Groome et al. 2001; Geen and
100 Canil, 2023). Seyler et al (2022) suggest the Leech River fault that bounds the forearc
101 sedimentary protolith of the Pacific Rim Terrane to the south was the interface of subcretion
102 (Fig. 1). The terrane was then exhumed by ~ 45 Ma as recorded by Ar-Ar ages of muscovite
103 (Groome et al. 2003).

104 ## Methodology

105 ### *Thermometry*

106 Metamorphic temperatures for the Pandora Peak Unit and Leech River Complex (Fig. 1)
107 have been determined by application of Raman spectroscopy of carbonaceous matter
108 geothermometry (T_{RSCM}) and garnet-biotite Fe-Mg exchange geothermometry and described in
109 detail in a prior study by Geen and Canil (2023). The T_{RSCM} on 23 individual samples from that

study are contoured over the field area (Figure 1) and used as a template of the metamorphic field gradient to view changes in sulfide behaviour and metal concentrations in the samples from this study.

Whole Rock Geochemistry

Rock samples of metapelites and metabasites were selected to assess S, C, and trace element content between protoliths and across metamorphic grade. Bulk rock major element geochemistry was determined on 13 samples. Trace element geochemistry including total S and C, were performed on a suite of 26 samples. Analyses were completed at Activation Laboratories Ltd. Major oxides were digested by lithium metaborate/tetraborate fusion, dissolved in 5% nitric acid, and analyzed by ICP-OES. Trace elements were analyzed by ICP-MS and INAA. Total C and S analyses were measured at Activation Laboratories Ltd via IR detection of SO_2 and CO_2 from 0.2 g of combusted sample material in a high oxygen environment. Results including detection limits and standards are given in Supplemental A1.

Electron Microprobe Analysis (EPMA) and Scanning Electron Microscopy (SEM)

Scanning electron microscopy was performed at the University of Victoria with a Hitachi S-48000 instrument to collect backscatter imagery of sulfide minerals. Qualitative identification of sulfides (pyrite, pyrrhotite, chalcopyrite, spahelerite, galena) in samples across the field area was performed using a Bruker Quantax EDS system with an accelerating voltage of 20 kV and current of 20 nA. Electron microprobe analyses for major and select trace elements in sulfides were performed on five samples at the University of Alberta using a JEOL JXA-8900R microprobe with the wavelength dispersive spectrometer (WDS) at an accelerating voltage of 20 kV and current of 20 nA (Supplemental A1). Spot analysis diameter was set to the minimum (1

μm) with 20 seconds on peak collection and 10 seconds on background collection for each analyte. Standards used are gallium arsenide (As), sphalerite (Zn). Pyrrhotite (Fe, S), alabandite (mn), copper metal (Cu) and nickel metal (Ni). Detection limits are given in Supplemental A1.

Phase Diagrams

Phase equilibrium diagrams for the metasedimentary units were generated using PerpleX (Connolly 2005). Bulk rock major element data for modelled samples were recast in the compositional system MnNCKFMASHTO+S (MnO-Na_2O-CaO-K_2O-FeO-MgO-Al_2O_3-SiO_2-H_2-O_2 – C and S_2), with C set as a saturated component to reflect conditions for graphitic metasediments without specification of fO_2 conditions. The bulk rock composition of a garnet-staurolite-sillimanite schist (AG080 - Table 1) was selected as a typical 'benchmark' pelite for the calculations. This composition is similar across metamorphic (chlorite to staurolite) grades in the Leech River Complex (Table 1). The 'benchmark' pelite AG080 composition (X1) is within ±10% relative of the median Si, Ti, Al and Fe and XMg of 5729 world pelite samples (Forshaw and Pattison, 2023), but has higher bulk Ca and Na (Table 1). More relevant to the model calculations of sulfide stability are the assumed bulk S content. The loss on ignition (LOI) value from bulk rock analyses was the initially assumed H_2O content. Because metamorphic temperature in the Pacific Rim Terrane is universally >200 °C (Geen and Canil, 2023), high grade schists such as AG080 in the Leech River Complex may have lost S, and a faithful record of pre-metamorphic S contents is unavailable. The S content in siliciclastic marine sediments commonly ranges from 0 to 2.5 wt% S, and total S is positively correlated with total organic carbon at C/S 2.8±0.8 (by weight) (Goldhaber, 2003). Applying this relationship to the C contents of carbonaceous pelites in the Leech River Complex and Pandora Peak Unit (Supplemental A1) gives total S contents of 0.25 – 1 wt% in their protolith. Based on this

155 estimate, 0.65 wt% S_2 was assumed in the benchmark pelite (AG080) bulk rock composition for
156 the initial model calculations.

157 Pressure-Temperature (P-T) diagrams were calculated from one to six kilobars and 300 –
158 700 °C. The thermodynamic dataset used is Holland and Powell (2011) for silicates , carbonates
159 and oxides. The thermodynamic data and solution models for sulfides are from Evans et al.
160 (2010). The solution models of White et al. (2014) were used for garnet, biotite, staurolite,
161 chlorite, epidote, white mica, ilmenite, and cordierite. The ternary feldspar solution model after
162 Fuhrman and Lindsley (1988) was utilized. The basic ideal stilpnomelane and four component
163 non-ideal carbonate solution models were also used. The selected chemical system excludes
164 many components relevant to sulfide phases (e.g., Cu, As, Ni) as solution models for these
165 components are not yet available. The fluid phase was treated explicitly as a solution using the
166 COHS fluid model, which relies upon equations of state for the pure species H_2O, CO_2, CO, H_2,
167 and H_2S (e.g., Connolly and Cesare 1993). To produce fluid-present conditions at low
168 temperatures (<350 °C) molar H_2O was artificially raised above the LOI value, while the ratios
169 of other components were unchanged.

170 **Results**

171 ***Sulfide Petrography***

172 Sulfides occur in 56 samples across the field area and are described with increasing
173 metamorphic temperature based on the isotherms in Figure 1. Detailed descriptions of the rocks
174 hosting the sulfides are given in Geen and Canil (2023). Our focus is on the sulfides hosted in the
175 matrix and porphyroblasts of the metasedimentary and metaigneous lithologies across grade in
176 the Pacific Rim Terrane. We do not consider the sulfide assemblages associated with the Au-

bearing quartz veins generally hosted in the thick metasandstone successions. The veins belong to a late hydrothermal or retrograde metamorphic paragenesis.

A summary of sulfide parageneses, metamorphic index mineralogy and temperatures are given in Table 1 and Figure 2. Among low grade argillites and clastic tectonites, Py commonly occurs as a framboidal morphology which can occur even in rocks which experienced substantial deformation, and attained temperatures up to ~350 °C (Fig. 3ab). Other common morphologies include euhedral to subhedral Py cubes. No sulfide is observed in all but the lowest grade metasandstones in which they typically form anhedral, "porous" Py grains. At comparable metamorphic temperatures along strike, disrupted radiolarian metachert from the Pandora Peak Unit hosts exclusively anhedral grains of Po with subsidiary chalcopyrite (Ccp) and rare grains of native Au.

Samples from medium metamorphic grades (350 – 450 °C), have a dearth of sulfide grains, but where they occur, Py is dominant. In one sample (AG105-1 – Table 1), thin "stringers" of Py occur parallel to the foliation, and thus likely represent primary grains deformed and recrystallized during prograde metamorphism. The Py stringers have a porous to poikiloblastic texture, an internal foliation-parallel fabric, and locally host small inclusions of Ccp (Fig. 3cde).

At higher grades (450 – 600 °C) the matrix sulfide assemblages are Py, Po, and Ccp. Sulfide grain morphology is highly variable, including deformed Py cubes, and elongated anhedral grains that are deformed in the foliation. The highest grade metapelites (575 – 600 °C) typically do not host any matrix sulfide. Porphyroblasts of andalusite, staurolite and garnet at high grades, interpreted to have formed between 575 and 600 °C (Geen and Canil, 2023), have inclusions of sulfides. The abundance of inclusions in andalusite varies from completely barren

to numerous at identical metamorphic temperatures. In one coarse andalusite porphyroblast, inclusions of coexisting Py and Po are observed (Fig. 4a,b). Therein the adjacent Py and Po grains are both angular and anhedral, but the former hosts numerous small silicate and Ccp inclusions distributed throughout the grain. Conversely, the adjacent Po hosts few silicate inclusions, and Ccp persists as larger round blebs at the grain margin (Fig. 4c). The Po inclusions elsewhere within the same porphyroblast host rounded silicate blebs, but Ccp always occurs either as independent adjacent grains (Fig. 4d) or rounded intergrowths propagating from grain margins (Fig. 4e). Staurolite porphyroblasts are highly poikiloblastic, often containing inclusions of Po and occasionally Py. Inclusion morphology within staurolite is comprising rounded anhedral and non-porous blebs. Garnet porphyroblasts are typically euhedral and < 0.5 mm diameter, and in some cases host small anhedral Po ± Ccp grains.

Metabasites interfoliated with metasedimentary rocks are observed across all metamorphic grades in the Leech River Complex and Pandora Peak Unit. Metabasites at low grade host irregular Py and Po as discrete grains and disseminated in deformed veins. Overall, in metabasite units Po is more abundant than Py at comparable metamorphic temperatures when compared to metasedimentary lithologies, although Py does locally occur as blebs within Po at moderate grade (~400 °C). High grade amphibolites are often sulfide-poor, or host trace amounts of Po and Ccp as inclusions in amphibole or grown in the interstices between laths. Metabasite lithologies which bear pink garnetite banding are associated with a greater modal abundance of interstitial Po locally replaced at the margins by fingers of bornite and an Fe-oxide (Fig. 3 f,g,h).

Bulk Rock Geochemistry

Bulk LOI values (mostly H_2O) decrease with increasing temperature in both metasediments and metabasites. The bulk C (as carbonaceous matter) in the pelites, likely

controlled by original variations in the protolith (Pattison, 2006) shows no trend with increased grade of metamorphism, whereas a decrease of bulk C (as carbonate) is observed in metabasites (Fig. 5a,b). Bulk S in both metasedimentary and metabasic lithologies show considerable variation across metamorphic temperatures (Fig. 5c) suggesting it too is controlled by original protolith concentrations. Chalcophile trace elements (Cu, Pb, Zn, As and Ga) do not exhibit systematic variation with metamorphic grade (Fig. 5d,e). Bulk Ni/Co exhibits a notable increase with metamorphic grade up to 400 °C among both metasedimentary rocks and metabasites (Fig. 5e,f). Most analyses for Au were below the 2 ppb detection limit (Supplemental A1). The three high-grade samples above detection limit are associated with prevalent late quartz veining in andalusite-bearing schists from the Valentine Mountain region.

Sulfide Chemistry

There are only four main sulfide phases throughout the sample suite, with Py and Po being the most common, followed by Ccp, and only trace sphalerite. A small subset of Py grains at low and high temperatures contain up to 0.05 wt % As. Appreciable Cu was only measured in Ccp grains or Py hosting micro-inclusions of Ccp. The Ni contents in Po are up to 0.75 wt% in metasedimentary samples, and up to 2.8 wt% in the metabasite sample analyzed. The Ni content in Py is more variable from below detection limit for grains in the matrix, up to 0.22 wt% among Py inclusions in andalusite.

The molar Fe/S values in Po show significant variation from ~0.83 to 0.92 across a temperature range of 300 to 600 °C (Fig. 6a). Much of the scatter is in the matrix phase. The Ni contents show a systematic decrease with metamorphic temperature in metapelites (Fig. 6b). The Fe/S and Ni contents of Po show a regular correlation to host porphyroblast phase (Fig. 6c,d). The Fe/S increases, and Ni decreases in pyrrhotite in the order of matrix, andalusite,

246 staurolite and garnet, the inferred mineral appearance with increasing grade in these rocks based
247 on textural and phase equilibrium considerations (Geen and Canil, 2023).

248 **Discussion**

249 ***Thermodynamic Modelling and Phase Diagrams***

250 We describe calculated phase diagrams along an isobaric path at 4 kbar expected for
251 metamorphism of the Leech River Complex (Geen and Canil, 2023) and then compare these with
252 natural assemblages. In the phase diagram for the benchmark composition X1, the Py-Po
253 transition occurs over < 5 °C and concludes by 390 °C (Fig. 7). The terminal chlorite-out
254 reaction occurs between ~480 and 540 °C. Thus, the Py-Po transition does not coincide with the
255 fluid release associated with chlorite breakdown for a typical Leech River Complex pelite. Other
256 studies have obtained similar results (Zhong et al. 2015).

257 The predicted phase abundances show that across the Py breakdown reaction, an increase
258 in the proportion of Po ($Fe_{1-x}S$) is accompanied by a concomitant decrease in the proportion of
259 stilpnomelane, the dominant Fe-bearing phase at temperatures below chlorite stability (Fig. 8).
260 Similarly, the proportions of quartz, fluid, and white mica increase across the Py breakdown
261 reaction. Sulfur liberated by Py breakdown produces additional Po by reacting with Fe in
262 stilpnomelane. Therefore, reaction [2] is largely inapplicable since reactions with silicate phases
263 sequester the released S (Zhong et al. 2015). The total Po content of the rock does not remain
264 constant above the Py breakdown reaction. Instead, ~0.13 vol% Po is lost between 370 °C and
265 600 °C, and there is a concomitant increase in fluid X_{H2S} content and the Fe/S ratio of remaining
266 Po (Fig. 8). From the initial Po formation T up to 600 °C, Fe/S ratios increase from ~0.91 to
267 ~0.94.

This is the peer-reviewed, final accepted version for American Mineralogist, published by the Mineralogical Society of America.
The published version is subject to change. Cite as Authors (Year) Title. American Mineralogist, in press.
DOI: https://doi.org/10.2138/am-2023-8973. http://www.minsocam.org/

The terminal chlorite breakdown reaction which occurs between 500 – 550 °C produces fluid, biotite, and staurolite (Fig. 8) indicative of the generalized, unbalanced reaction:

$$Chl + Mu + Pl = Bt + St + Pl + H_2O \quad [3]$$

Across this reaction, the slope of Po consumption is steepened, and there is a corresponding step increase in fluid X_{H2S}. Simultaneously, the Fe/S of Po abruptly decreases before resuming monotonic increase with progressive heating. Therefore, the devolatilization accompanying terminal chlorite breakdown in turn drives the breakdown of Po in response to a decrease in fluid X_{H2S} from adding water-rich fluid.

Because the Leech River Complex comprises numerous metasedimentary protoliths that are sometimes interfoliated on the centimeter scale, we evaluated the sensitivity of the Py-Po transition to various bulk compositions using temperature-composition (T-X) sections. The compositional variables assessed are FeO, CaO, bulk S, and the extent of metapsammitic lithologies (bulk SiO_2) mixed in the metapelites of the Leech River Complex.

Variable Psammite Fraction in Protolith

At 4 kbar, the change from metapelitic (X1) to metapsammitic (X2) lithologies predicts an expansion of Py to ~415 °C, and lowering of the temperature for first appearance of Po at ~350 °C (Fig. 9a). The temperature of the chlorite breakdown reaction remains > 540 °C for ~80 percent of the compositional variation from metapelite to metapsammite, but dramatically decreases in Fe-poor psammitic compositions. At 4 kbar in the metapsammitic composition X2, the terminal chlorite breakdown reaction is lowered to ~440 °C, and chlorite is not produced until ~420 °C, and its predicted modal volume never exceeds 1% (Fig. 9a). Similarly, the chlorite terminal breakdown reaction is shifted to below 540 °C, but any significant fluid generation via

This is the peer-reviewed, final accepted version for American Mineralogist, published by the Mineralogical Society of America.
The published version is subject to change. Cite as Authors (Year) Title. American Mineralogist, in press.
DOI: https://doi.org/10.2138/am-2023-8973. http://www.minsocam.org/

chlorite breakdown occurs at conditions much above the calculated Py-Po reaction. Thus, metapsammitic lithologies widen the Py-Po window, but not sufficiently to coincide with the terminal chlorite breakdown reaction and any associated release of fluid (Tomkins 2010).

Variable FeO

Adjustment of total molar FeO by ± 50% relative of the X1 benchmark composition (Fig. 9b) shows that this parameter is a dominant control on Py breakdown in the metapelite-metapsammite section. Reduction of molar FeO (i.e., bulk FeO from 7 to 3.5 wt%) produces a similar effect to variation towards a psammitic lithology, increasing the first appearance of Po by ~40 °C. Therefore, the field of coexisting Py and Po expands in a bulk rock composition comprising significantly lower molar FeO, such as the metapsammitic composition X2 or the low-FeO case X4 (Fig. 9b). Conversely, isobaric paths for sections with up to 50% additonal molar FeO were characterized by narrowing the Py breakdown reaction, and the conversion of Py to Po at conditions below <300 °C (Fig. 9b.

The substantial variation in bulk rock FeO among metasedimentary rocks in the Pacific Rim Terrane due to cm- to m-scale layering of metapsammite within metapelite successions could cause local variability in the exact temperature Py breakdown, as has been reported in the Otago Schist in New Zealand (Pitcairn et al. 2010). However, the section for variable FeO (Fig. 9b) was prescribed at constant bulk S_2 content of 0.5 mol % to isolate the influence of changing FeO.

Variable CaO

Limestone horizons have been reported in the Pacific Rim Terrane (e.g., Fairchild and Cowan 1982). Thus, the effect of bulk rock CaO content may also bear on the conditions of Py breakdown. The constructed T-X section is for an increase in molar CaO by a factor of four to

simulate carbonate-bearing metasedimentary rocks (Fig. 9c). At higher CaO contents, the first appearance of chlorite on a prograde path is shifted to temperatures above the Py-Po transition. and the first appearance of biotite is reduced to <400 °C. For the maximum CaO composition, chlorite is only stable over a <20 °C (Fig. 9c). Thus, for carbonate-bearing metasedimentary rocks the prograde breakdown of chlorite produces much less fluid than in the typical metapelites. The maximum stability of Py is approximately unchanged for CaO-rich compositions, remaining <350 °C at 4 kbar but the width of the Py-Po transition is widened.

Variable S Content

The stability of Py and Po is dependent on the S content of the system (Tomkins, 2010; Evans et al. 2010), and greater proportions of Py versus Po occur in rocks with greater molar S/Fe (Ferry 1981). Although 0.5 mol% S_2 (0.65 wt%) was selected for as an initial point for the calculations, the sedimentary lithologies and low-grade samples from the Pacific Rim Terrane can have locally heterogeneous distributions of primary sulfide. The effect of variable S_2 content on the Py-Po transition was investigated by varying the benchmark composition from 0.1 mol % to 5.0 mol % S_2 (Fig. 10) at 4 kbar. The appearance of Po is shifted to higher temperatures with increasing S content. Conversely, at specified S contents less than the benchmark X1 case, the transition is narrow and low until ~0.25 mol % S_2. Below this level of S, Po is stabilized and Py entirely destabilized at temperatures below the section domain.

Over the range 0.25 – 1.6 mol % S_2, which encompasses most sulfide-bearing metapelites, the effect of bulk S_2 is limited to a gradual widening of the Py-Po transition. Above ~1.6 mol % S_2, Py is stabilized to drastically higher temperatures until at ~2.8 mol % S_2 the appearance of biotite coincides with Py-out (Fig. 10). Above 3 mol % S_2 the Py-Po reaction co-exists with chlorite breakdown. Thus, the “ideal” case for simultaneous fluid production via

This is the peer-reviewed, final accepted version for American Mineralogist, published by the Mineralogical Society of America.
The published version is subject to change. Cite as Authors (Year) Title. American Mineralogist, in press.
DOI: https://doi.org/10.2138/am-2023-8973. http://www.minsocam.org/

chlorite breakdown and S release via the Py-out reaction occurs in samples containing > 3 mol % S_2, wherein both reactions occur in a narrow window at ~540 °C. Few typical marine siliciclastic sediments contain > 1 mol% S_2 (Goldhaber 2003). Therefore, while S_2 content is the most influential parameter on the Py-Po transition (even above FeO variations), only exceptional and localized protoliths such as hydrothermal sediments or pyrite lenses could result in alignment of both the Py -Po and chlorite-breakdown reactions in the equilibrium phase diagram. On a more regional scale, variations in FeO within metapelite successions are more likely to change in the temperature of Py breakdown.

Comparison of models with metasedimentary rocks

Low Grade

The calculated phase diagrams can be compared with natural assemblages. Argillite and phyllite from the Leech River Complex do not show most of the predicted model assemblages in the X1 benchmark phase diagram at low grade below the chlorite isograd. For example, among carbonaceous phyllite, sphene grains are observed, but the volumes of stilpnomelane, garnet, paragonite and epidote predicted in the model are not. Silicate phases formed above the chlorite-in reaction are more compatible with mineralogy in the rocks (Figs. 2, 7).

Regarding sulfides, metasedimentary rocks from the Pandora Peak Unit and a small subset of the Leech River Complex that attained temperatures less than 300 °C show Py that retains some primary and diagenetic textures (Fig. 2). Thus, samples which correspond to temperatures below the modelled temperature domain are consistent with Py being the dominant pre-metamorphic sulfide, and its retention to sub-greenschist conditions in other thermodynamic models and in natural rocks (e.g., Carpenter 1974; Tomkins 2010; Pitcairn et al. 2010).

This is the peer-reviewed, final accepted version for American Mineralogist, published by the Mineralogical Society of America.
The published version is subject to change. Cite as Authors (Year) Title. American Mineralogist, in press.
DOI: https://doi.org/10.2138/am-2023-8973. http://www.minsocam.org/

Rocks with temperatures between 300 and 400 °C exhibit more varied incompatibility with the predictions of the model phase diagrams. While Py still occurs in this range, several samples comprise Po-dominated assemblages (Table 1, Fig. 2). For example, Sample AG010 from the Pandora Peak Unit attained peak temperatures of ~300 °C but contains Po (Fig. 9). The presence of Po in sub-greenschist facies occurs in comparable metamorphic terranes of the Otago and Alpine schists, where it is the main sulfide among sub-greenschist facies rocks (Pitcairn et al. 2010). Conversely, the Barrovian-type Ocoee Series has a distinct Po isograd that occurs slightly downgrade of the biotite isograd (Carpenter 1974). Therefore, Po stability at temperatures of ~300 °C is inconsistent with the model predictions. Conversely, the Py stringers from sample AG105-1 (Fig. 3) are interpreted as pre-metamorphic Py subject to concomitant deformation and metamorphism. The protolith composition is comparable to the benchmark pelite, and thus at a temperature of 400 °C and 4 kbar, the predicted stable sulfide in should be Po (Figs. 7, 8).

High Grade

In upper greenschist and amphibolite facies rocks, Py remains a prevalent matrix phase in the Leech River Complex schists. Most matrix Py grains are anhedral, and are generally interpreted here as part of retrograde assemblages. For these reasons, inclusion assemblages among the common porphyroblasts provide the least ambiguous record of sulfide stability during prograde metamorphism since they are isolated from ongoing equilibration with the matrix and metamorphic fluids (Brown et al. 2014). Textures suggests the generalized sequence of porphyroblast formation in the Leech River pelites is: (1) andalusite (in sufficiently aluminous protoliths), (2) staurolite on or embaying rims of andalusite, and (3) garnet growing coincidental with staurolite (Geen and Canil, 2023). These textural features may be interpreted to reflect

nearly coincident growth of all three minerals over a narrow temperature range, possibly catalysed by fluid in a 'cascade effect' (Pattison and Tinkham, 2009).

The occurrence of Py inclusions in andalusite and staurolite porphyroblasts (Fig. 3) as isolated and composite grains with Po is clearly above the Py breakdown reaction in the model (Figs. 7, 11). In the model, staurolite can be a product of chlorite and muscovite breakdown at > 540 °C, suggesting Py was included by these porphyroblasts above this temperature (Fig. 7). The occurrence of staurolite and andalusite assemblages in rocks frequently do not agree with predictions of thermodynamic models for kinetic reasons (Pattison and Spear, 2018). Overstepping is required to form porphryoblasts and displaces their occurrence in natural rocks by upward of 30 to 70 °C compared to calculated phase diagrams (Pattison and Tinkham, 2009; Spear and Pattison, 2017). Nevertheless, staurolite formation at > 540 °C in the phase diagram (Fig. 7) is consistent with T_{RSCM} > 530°C for samples in which it occurs (Table 1, Fig. 2; Geen and Canil 2023) suggesting Py was overgown by this phase at these temperatures. Conversely, garnet porphyroblasts never host Py. Garnet-biotite Fe-Mg exchange geothermometry indicates that garnet containing Po forms near peak temperature conditions (550 - 600°C) (Geen and Canil, 2023). A caveat in comparison of the garnet-hosted sulfide assemblages with other porphyroblasts is the significant discrepancy in grain size: staurolite and andalusite locally form grains in excess of one centimeter, while garnet in most samples is <0.5 mm.

Sulfide mineral assemblages among the Leech River Complex and Pandora Peak Unit can be generalized by a greater frequency of Po and chalcopyrite (Ccp) among high grade rocks (>500 °C), and Py occurring across grade and exhausted by 550 °C. Pyrite in natural rocks greatly exceeds conditions of its stability, and of fluid release (chlorite-out), predicted in the calculated phase diagrams (Fig. 11). At lower temperatures the comparison of prograde changes

This is the peer-reviewed, final accepted version for American Mineralogist, published by the Mineralogical Society of America.
The published version is subject to change. Cite as Authors (Year) Title. American Mineralogist, in press.
DOI: https://doi.org/10.2138/am-2023-8973. http://www.minsocam.org/

in the sulfide assemblage with models is somewhat obscured by the paucity of sulfides in upper greenschist facies phyllites. Field observations suggest that this gap is not an artefact of sampling, but that bulk rock S simply varied in original protolith compositions (Fig. 5c). While the mobilization of S at higher temperatures (> 550 °C) is not evident in whole rock S contents (Fig. 5c) it is clearly captured by the systematic increase in Fe/S in Po included in porphyroblasts occurring with increasing grade from andalusite < staurolite < garnet (Fig. 7d).

If S liberated from Py breakdown does not react with Fe-silicates to produce additional Po, as predicted in our models, it is possible that X_{H2S} (fluid) is higher (e.g., Ferry 1981), and there is less modal Po than predicted by the models. Alternatively, if unlike the presented closed-system models (Fig. 7 – 10), there is continual export of fluid with the liberated S and replenishment by new fluid from the breakdown of hydrous minerals, a net loss of S could be incurred.

The Equilibrium Assumption

Limitations of applying the calculated phase diagrams to physical samples are the selection of a representative bulk chemistry, the scale of the equilibration volume (Palin et al. 2016; Lanari and Engi 2017) and equivocally demonstrating attainment of equilibrium (Connolly 2005). The equilibrium assumption amongst all components in a rock is not met throughout the greenschist facies (Carlson 2002). The effect of the equilibration or 'reactive' bulk composition (Lanari and Engi 2017) may also bear significantly on sulfide stability. The width of the Py-Po transition is highly sensitive to bulk S_2 (Fig. 10), and to a lesser degree, FeO (Fig. 9b). While S_2 comprises generally less than 1 mol% in the bulk analysis of a fist-sized metapelite sample, the 'reactive' bulk composition on a smaller scale could comprise proportionally more sulfide. Increasing specified S_2 to 4 mol% of the bulk composition widens Py stability to T above

terminal chlorite breakdown (Fig. 10). There is also evidence for restrictive local equilibrium among comparable graphitic metasediments. Strongly heterogeneous $\delta^{34}S$ values inherited from pre-metamorphic sulfide can persist on the cm-scale in medium-grade metamorphism of rocks for which the scales of isotopic equilibrium have are estimated to be tens or hundreds of meters (Oliver et al. 1992).

Orogenic Gold Deposits

Fluid loss and net transfer of S and Au by Py breakdown during prograde metamorphism is a process central to the metamorphic orogenic Au model (Tomkins 2010) . In metasedimentary lithologies of forearcs, high-temperature low-pressure metamorphism is commonly associated with quartz-sulfide hosted Au ore deposits (Haeussler et al. 1995; Pitcairn et al. 2006; 2010). In the Pacific Rim Terrane, the Leech River Complex hosts the Valentine Mountain Au deposit (Fig. 1). The phase diagrams of this study for metamorphism of sulfide-bearing carbonaceous sediments in the Pacific Rim Terrane (Figs. 7-10) show that Py breakdown could occur along different temperatures in different protoliths, depending on their bulk S, Fe and psammitic contents. While rock data show a loss of fluid (mostly as H_2O) with increasing metamorphic grade (Fig. 5a) a monotonic decrease in total S contents is not evident between 300 and 600 °C (Fig. 5c). The changes in Fe/ S at highest grades indicated by sulfide porphyroblasts (Fig. 6d) are a reasonable indication that some open-system S loss occurred, yet all of Cu, Zn, Ga, and Pb show indistinct changes in the bulk rock at these conditions (Fig. 5), as is also observed at 500 to 650 °C in the classic Ballacullish contact aureole (Finch and Tompkins 2017). Unfortunately, Au is only detected among very low- or high-grade samples (Supplemental A1) but if it behaviour follows As (Fig. 5e) there is no obvious concomitant mobility of these two metals during prograde metamorphism of the forearc sediments represented by the Leech River and

Pandora Peak units. Thus, evidence is lacking that Py breakdown and concomitant S loss drove any mobilization chalcophiles to produce orogenic Au deposits in the Pacific Rim Terrane.

Implications

The equilibrium model phase equilibria for Py breakdown conflicts with petrographic evidence of forearc metasediments of the Pacific Rim Terrane, which indicates that Py co-exists with Po up to 550 °C, far higher than is suggested by models (Fig. 11). Calculated phase diagram models of the low temperature phase equilibria are suspect, and samples from low greenschist facies conditions (< 400 °C) may represent only partial or local equilibrium. The spatial scale of equilibration and processes governing the Py breakdown reaction at low grades could be tested more rigorously by thin-section scale evaluation of δ^{34}S values in greenschist facies rocks. If the reactive bulk volumes are indeed small (cm-scale) in sub-amphibolite facies metamorphism, future thermodynamic modelling should consider the prospects of S comprising a greater proportion of the reactive bulk chemistry, as well as the effects of the net export of S via metamorphic fluid from the system during devolatilization of metapelites. In this case, the S may comprise a much greater proportion of the effective bulk composition in a reaction than that estimated for a homogenized metasedimentary sample. This widens the T interval that Py and Po may coexist throughout greenschist and lower amphibolite facies. The pyrrhotite compositions in andalusite, staurolite and garnet porphyroblasts from the Pacific Rim Terrane show net mobilization of S at highest metamorphic grades, but the process is not necessarily connected to any local Au deposits.

Acknowledgements - We thank D. Fode for field assistance and A. Locock for help with the EPMA analyses (U. Alberta). We appreciate an extremely helpful review by D. Pattison and D. Dolejs for editorial handling. This research was funded by a Society of Economic Geologists Student Grant and NSERC of Canada Scholarship to AG, and a NSERC of Canada Discovery Grant (154275) to DC.

References

Canil, D., and Fellows, S. A. (2017) Sulphide–sulphate stability and melting in subducted sediment and its role in arc mantle redox and chalcophile cycling in space and time. Earth and Planetary Science Letters, 470, 73-86. https://doi.org/10.1016/j.epsl.2017.04.028

Carlson, W. D. (2002) Scales of disequilibrium and rates of equilibration during metamorphism. American Mineralogist, 87, p.185–204. https://doi.org/10.2138/am-2002-2-301

Carpenter, R. H. (1974) Pyrrhotite isograd in southeastern Tennessee and southwestern North Carolina. Geological Society of America Bulletin v.85, 451–456. https://doi.org/10.1130/0016-7606(1974)85<451:PIISTA>2.0.CO;2

Connolly, J. A. D. (2005) Computation of phase equilibria by linear programming: A tool for geodynamic modeling and its application to subduction zone decarbonation. Earth and Planetary Science Letters, 236, 524–541. https://doi.org/10.1016/j.epsl.2005.04.033

Connolly, J.A.D., and Cesare, B. (1993) C-O-H-S fluid composition and oxygen fugacity in graphitic metapelites. Journal of Metamorphic Geology, 11: 379-388. https://doi.org/10.1111/j.1525-1314.1993.tb00155.x

Cui, Y., Miller, D., Schiarizza, P., and Diakow, L.J. (2017) British Columbia digital geology. British Columbia Ministry of Energy, Mines and Petroleum Resources, British Columbia Geological Survey Open File 2017-8, 9 Data version 2019-12-19.

Evans, K. A., Powell, R., and Holland, T. J. B. (2010) Internally consistent data for sulphur-bearing phases and application to the construction of pseudosections for mafic greenschist facies rocks in Na2O-CaO-K2O-FeO-MgO-Al2O3-SiO2-CO2-O-S-H2O: Internally

consistent data for sulphur-bearing phases. Journal of Metamorphic Geology, 28, 667–687. https://doi.org/10.1111/j.1525-1314.2010.00890.x

Evans, K.A., and Tomkins, A.G. (2011) The relationship between subduction zone redox budget and arc magma fertility. Earth and Planetary Science Letters, 308, 401-409. https://doi.org/10.1016/j.epsl.2011.06.009

Fairchild, L. H., and Cowan, D. S. (1982) Structure, petrology, and tectonic history of the Leech River complex northwest of Victoria, Vancouver Island. Canadian Journal of Earth Sciences, 19, 1817–1835. https://doi.org/10.1139/e82-161

Forshaw, J.B., and Pattison, D.R.M.(2023) Major-element geochemistry of pelites: Geology, 51, 39–43, https://doi.org/10.1130/G50542.1

Ferry, J.M. (1981) Petrology of graphitic sulfide-rich schists from South-central Maine: an example of desulfidation during prograde regional metamorphism. American Mineralogist, v.66, p.908–930.

Finch, E. G., and Tomkins, A. G. (2017) Pyrite-pyrrhotite stability in a metamorphic aureole: Implications for orogenic gold genesis. Economic Geology, v.112, 661–674. https://doi.org/10.2113/econgeo.112.3.661

Fuhrman, M.L., and Lindsley, D.H. (1988) Ternary-feldspar modeling and thermometry. American Mineralogist, 73, 201–215.

Geen, A.C. (2021) High temperature forearc metamorphism and consequences for sulfide stability in the Pacific Rim Terrane, British Columbia. Unpublished MSc Thesis, University of Victoria, Canada.

518 Geen, A. C., and Canil, D. (2023) Pattern and source of unusually high-temperature
519 metamorphism in an Eocene forearc recorded by the Pacific Rim Terrane, British Columbia,
520 Canada. Journal of Metamorphic Geology, 1–20. https://doi.org/10.1111/jmg.12709

521 Goldhaber, M. B. (2003) Sulfur-rich Sediments. In Treatise on Geochemistry, Volume 7.
522 Editors: Holland, H.D., Turekian, K.K. Pergamon. , 257–288. https://doi.org/10.1016/B0-08-
523 043751-6/07139-5

524 Groome, W. G., Thorkelson, D. J., Friedman, R. M., Mortensen, J. K., Massey, N. W. D.,
525 Marshall, D. D., and Layer, W. (2003) Magmatic and tectonic history of the Leech River
526 Complex, Vancouver Island, British Columbia: Evidence for ridge-trench intersection and
527 accretion of the Crescent Terrane. In B. Sisson, S. M. Roeske, and T. L. Pavlis, Geology of a
528 transpressional orogen developed during ridge-trench interaction along the North Pacific
529 margin. Geological Society of America. https://doi.org/10.1130/0-8137-2371-X.327

530 Grove, E.W. (1984) Geological report and work proposal on the Valentine Mountain Property,
531 Assessment Report 12642, NTS 92B/12W. Retrieved from:
532 https://aris.empr.gov.bc.ca/search.asp?mode=repsumandrep_no=12642

533 Groves, D.I, Goldfarb, R. J., Gebre-Mariam, M., Hagemann, S. G., and Robert, F. (1998)
534 Orogenic gold deposits: A proposed classification in the context of their crustal distribution
535 and relationship to other gold deposit types. Ore Geology Reviews, 13, p.7–27.
536 https://doi.org/10.1016/S0169-1368(97)00012-7

537 Haeussler, J., Bradley, D., Goldfarb, R., Snee, L., and Taylor, C. (1995) Link between ridge
538 subduction and gold mineralization in southern Alaska. Geology, 23, 995–998.
539 https://doi.org/10.1130/0091-7613(1995)023<0995:LBRSAG>2.3.CO;2

Hammerli, J., Spandler, C., and Oliver, N. H. S. (2016) Element redistribution and mobility during upper crustal metamorphism of metasedimentary rocks: An example from the eastern Mount Lofty Ranges, South Australia. Contributions to Mineralogy and Petrology, 171, https://doi.org/10.1007/s00410-016-1239-7

Holland, T. J. B., and Powell, R. (2011). An improved and extended internally consistent thermodynamic dataset for phases of petrological interest, involving a new equation of state for solids. Journal of Metamorphic Geology, 29, 333–383. https://doi.org/10. 1111/j.1525-1314.2010.00923.x

Houle, J. (2011) Technical Report on the Valentine Mountain Property, Assessment Report 32500, NTS 092B12W. https://aris.empr.gov.bc.ca/search.asp?mode=repsumandrep_no=32500

Jakob, J., Johnston, S. T., Beyssac, O., and Corfu, F. (2016) The structural evolution of the Leech River Complex, Vancouver Island, Canada: in Geodynamic Significance of Regional Melange Units at Divergent and Convergent Plate Margins, Jakob, J. Doctoral Dissertation. University of Oslo, Norway.

Lanari, P., and Engi, M. (2017) Local bulk composition effects on metamorphic mineral assemblages. Reviews in Mineralogy and Geochemistry. 83: 55–102. doi: https://doi.org/10.2138/rmg.2017.83.3

Large, R., Thomas, H., Craw, D., Henne, A., and Henderson, S. (2012) Diagenetic pyrite as a source for metals in orogenic gold deposits, Otago Schist, New Zealand. New Zealand Journal of Geology and Geophysics, 55, 137–149. https://doi.org/10.1080/00288306.2012.682282

562 Oliver, N.H.S., Hoering, T.C., Johnson, T.W., Rumble III, D., and Shanks III, W.C. (1992)
563 Sulfur isotopic disequilibrium and fluid-rock interaction during metamorphism of sulfidic
564 black shales from the Waterville-Augusta area, Main, USA. Geochimica et Cosmochimica
565 Acta, 56, 4257 – 4265. https://doi.org/10.1016/0016-7037(92)90266-L

566 Palin, R. M., Weller, O.M., Waters, D.J., and Dyck, B. (2016) Quantifying geological
567 uncertainty in metamorphic phase equilibria modelling; a Monte Carlo assessment and
568 implications for tectonic interpretations. Geoscience Frontiers, 7, 591-607.
569 https://doi.org/10.1016/j.gsf.2015.08.005

570 Pattison D.R.M. (2006) The fate of graphite in prograde metamorphism of pelites: An example
571 from the Ballachulish aureole, Scotland. Lithos, 88, 85-99.

572 Pattison D.R.M., and Tinkham, D. (2009) Interplay between equilibrium and kinetics in prograde
573 metamorphism of pelites: an example from the Nelson aureole, British Columbia. Journal of
574 Metamorphic Geology, 27, 249–279.

575 Pattison D.R.M., and Spear F.S. (2018) Kinetic control of staurolite–Al_2SiO_5 mineral
576 assemblages: Implications for Barrovian and Buchan metamorphism. Journal of
577 Metamorphic Geology, 36, 667 -690. https://doi.org/10.1111/jmg.12302

578 Pitcairn I.K., Teagle, D.A.H., Craw, D., Olivo, G.R., Kerrich, R., and Brewer, T.S. (2006)
579 Sources of metals and fluids in orogenic gold deposits: Insights from the Otago and Alpine
580 Schists, New Zealand. Economic Geology, 101, 1525–1546.
581 doi.org/10.2113/gsecongeo.101.8.1525

582 Pitcairn, I.K., Olivo, G.R., Teagle, D.A.H., and Craw, D. (2010) Sulfide evolution during
583 prograde metamorphism of the Otago and Alpine Schists, New Zealand. The Canadian
584 Mineralogist, 48 , p.1267–1295. https://doi.org/10.3749/canmin.48.5.1267

585 Pitcairn, I.K., Skelton, A. D. L., and Wohlgemuth-Ueberwasser, C. C. (2015) Mobility of gold
586 during metamorphism of the Dalradian in Scotland. Lithos, 233, 69–88.
587 https://doi.org/10.1016/j.lithos.2015.05.006

588 Pokrovski, G. S., Tagirov, B. R., Schott, J., Hazemann, J.-L., and Proux, O. (2009) A new view
589 on gold speciation in sulfur-bearing hydrothermal fluids from in situ X-ray absorption
590 spectroscopy and quantum-chemical modeling. Geochimica et Cosmochimica Acta, 73,
591 5406–5427. https://doi.org/10.1016/j.gca.2009.06.007

592 Rusmore, M. E., and Cowan, D. S. (1985) Jurassic–Cretaceous rock units along the southern
593 edge of the Wrangellia terrane on Vancouver Island. Canadian Journal of Earth Sciences. 22,
594 1223-1232. https://doi.org/10.1139/e85-124

595 Seyler, C. E., Kirkpatrick, J. D., Faber, C., Licht, A., Šilerová, D., and Regalla, C. (2022)
596 Structural and metamorphic history of the Leech River Shear Zone, Vancouver Island,
597 British Columbia. Tectonics, 41, e2021TC007132. https://doi.org/10.1029/2021TC007132

598 Spear, F.S, and Pattison, D.R.M. (2017) The implications of overstepping for metamorphic
599 assemblage diagrams (MADs). Chemical Geology, 457, 38-46.

600 Stepanov, A. S. (2021) A review of the geochemical changes occurring during metamorphic
601 devolatilization of metasedimentary rocks. Chemical Geology, 568, 120080.
602 https://doi.org/10.1016/j.chemgeo.2021.120080

603 Thomas, H. V., Large, R. R., Bull, S. W., Maslennikov, V., Berry, R. F., Fraser, R., Froud, S.,
604 and Moye, R. (2011) Pyrite and pyrrhotite textures and composition in sediments, laminated
605 quartz veins, and reefs at Bendigo Gold Mine, Australia: Insights for Ore Genesis. Economic
606 Geology, 106, 1–31. https://doi.org/10.2113/econgeo.106.1.1

607 Tomkins, A. G. (2010) Windows of metamorphic sulfur liberation in the crust: Implications for
608 gold deposit genesis. Geochimica et Cosmochimica Acta, 74, 3246–3259.
609 https://doi.org/10.1016/j.gca.2010.03.003

610 Tomkins, A.G., and Evans, K.A. (2015) Separate zones of sulfate and sulfide release from
611 subducted mafic oceanic crust. Earth and Planetary Science Letters, 428, 73-83.
612 https://doi.org/10.1016/j.epsl.2015.07.028

613 Walters, J.B., Cruz-Uribe, A.M., and Marschall, H.R. (2020) Sulfur loss from subducted altered
614 oceanic crust and implications for mantle oxidation. Geochemical Perpsectives Letters 13,
615 36–41. https://doi.org/10.7185/geochemlet.2011

616 White, R.W., Powell, R., Holland, T.J.B., Johnson, T.E., and Green, E.C.R. (2014) New mineral
617 activity–composition relations for thermodynamic calculations in metapelitic systems.
618 Journal of Metamorphic Geology, 32, 261-286. https://doi.org/10.1111/jmg.12071

619 Zhong, R., Brugger, J., Tomkins, A. G., Chen, Y., and Li, W. (2015) Fate of gold and base
620 metals during metamorphic devolatilization of a pelite. Geochimica et Cosmochimica Acta,
621 171, 338–352. https://doi.org/10.1016/j.gca.2015.09.013

622

Figure Captions

Fig. 1 – (a) Geologic map of the Pacific Rim Terrane (PRT) on southern Vancouver Island, British Columbia, Canada (inset), showing the Leech River Complex (light grey) and Pandora Peak Unit (dark grey) modified after Cui et al (2017). The Pacific Rim Terrane is in fault contact with Wrangellia to the north along the San Juan Fault and underthrust by the Crescent-Siletz terrane to the south along the Leech River Fault. Also shown are Eocene and younger Carmanah Group sedimentary rocks, relevant major faults and various felsic (pink) and basic (green) metaigneous rocks. Samples used in this study are labelled and show locations of metamorphic temperatures measured using Raman Spectroscopy of carbonaceous matter (TRSCM) and garnet biotite FeMg exchange (TGtBt) (red diamonds, hexagons – (Geen and Canil, 2023); yellow diamonds – (Jakob et al, 2016) (b) Simplified isotherm map of the Pacific Rim Terrane that integrates the metamorphic temperatures in metasedimentary and metabasic rocks from (a). Areas with '?' were inaccessible. The red star shows location of the Valentine Mountain Au deposit (Houle, 2011).

Fig. 2 – Sulfide assemblages in samples from this study compared with metamorphic temperatures and index mineralogy for the Pacific Rim Terrane (Table 1 and Geen and Canil, 2023).

Fig. 3 – Petrographic images of sulfides from Pacific Rim Terrane . (a, b) Reflected light images of tectonized metasediment from the Pandora Peak Unit (DC0514) rich in carbonaceous matter (CM) showing disaggregated Py framboids and coarser Py aggregates (c) Polished mount of carbonaceous phyllite AG105-1with inset boxes corresponding to images in (d) and (e) . Deformed pyrite stringers have variable pitting textures, and can show foliation-parallel internal fabrics defined by microcrystalline inclusions. Large vertical fractures are indicative of brittle

646 extension. (f, g, h) Po grains surrounded by halos of bornite in metabasite (garnet amphibolite
647 sample AG069).

648 Fig. 4 – Transmitted light image of inclusions within a coarse andalusite porphyroblast in sample
649 AG042 with insets corresponding to backscattered electron images of (a) to (e). (a) Small,
650 anhedral Po inclusions with few silicate inclusions. (b) Large Po-Py composite grain, where Py
651 forms as blebby grains in Po margins. (c) Po grain with elongate Ccp lamellae possibly from
652 exsolution. (d) Coarse, fractured Po with ragged margins (rimmed by f.g. micas). (e)
653 Coexisting Py and Po in mutual contact. In Po, Ccp occurs as blebs arranged at the grain margin.
654 In Py, Ccp occurs as small point grains throughout along with small silicate inclusions.

655 Fig. 5 – Bulk rock element trends of metasediment and metabasite samples compared with their
656 metamorphic temperatures from T_{RSCM} (Figure 1). A. Loss on ignition B. bulk C (ppm) C. bulk S
657 (ppm) D. Cu E. As and F. Ni/Co. Other chalcophile elements (Pb, Zn, Ga) with no trends are
658 not shown (see Supplemental A1 for data).

659 Fig. 6 - Variations in A. molar Fe/S, molar M/S where M = (Fe + Ni + Zn), and B. Ni wt% in
660 pyrrhotite (Po) with increasing metamorphic temperature recorded by Raman Spectrosocpy of
661 Carbonaceous Matter (Geen and Canil 2023). Note AG137 (hexagon) is a metabasic actinolite
662 schist, whereas the other four samples are pelitic protoliths. Dashed line insets show the samples
663 plotted in panels C. and D. Values of C. Ni wt% and D. molar Fe/S in Po hosted in matrix and
664 andalusite, staurolite and garnet porphryroblasts, the order of mineral appearance with increasing
665 grade inferred by textural and phase equilibrium criteria. Uncertainties in all panels are one
666 standard deviation of the mean.

Fig. 7 – Calculated phase diagram of the typical 'benchmark' Leech River pelite bulk composition X1 (sample AG080 – Supplemental A1). Some field labels omitted for clarity. Key mineral -in and -out boundaries are highlighted, including Po-in, Py-out, Chl-in, and Chl-out. These lines represent the appearance or disappearance of mineral, either by a continuous reaction or discontinuous reaction. Lines A. and B. correspond to example isobaric heating paths at two different pressures.

Fig. 8 - Panel plots showing changes to mineral volumes and chemistry along isobaric heating path at 4 kbar from phase diagram of Figure 7. From left to right: (i) Volume percent of Py and Po across the Py breakdown threshold, and the terminal chlorite breakdown reaction boundary. (ii) Composition change in Po (Fe/S) recorded on left hand axis, including Fluid XH_2S on the right ($\times 10^{-3}$). As Po breaks down, the released S is accommodated in the fluid. (iii) Changes in mineral volume, and total fluid volume, with progressive isobaric thermal metamorphism

Fig. 9 - Temperature – Composition (T-X) phase diagrams at 4 kbar varying between the benchmark composition X1 of Figure 7 and other components. (a) phase diagrams of X1 with a more psammitic component (X2). Chlorite volume percent contours show the terminal chlorite breakdown reaction at high temperature, while the Py-Po transition remains <420 °C. (b) Phase diagrams of X1 with X3 having 50% (relative) less FeO, and X4 having 50% more FeO, and with fluid and bulk S_2 content adjusted to be constant. Reducing the FeO content increases the maximum temperature of Py-stability (c) Phase diagrams of X1 with a Ca-rich pelite. Higher CaO contents lead to a widening of the Py-Po transition to lower temperatures, below the model domain. Some stability field labels are omitted for clarity on the phase diagrams.

Fig. 10 - P-T phase diagrams for the bulk composition X1 renormalized for variable amounts of bulk S_2. The width and minimum temperatures of Py breakdown (black arrow) increase with

690 increasing bulk S_2 content. Note that at 4.0 mol% S_2 the Py-Po transition eclipses the terminal
691 chlorite breakdown reaction (shown schematically as the 'chl-out' field). The Py-Po transition
692 widens to a greater degree at higher S_2 values.

693 Fig. 11 - Histogram plot showing the distribution of the samples at their estimated peak
694 metamorphic temperature. (a) Sulfide-bearing samples (*) are defined as those which show
695 sulfide identified in hand sample, polished mount and thin section. Fields of 'desulfidation' and
696 'chl-out' indicate locations of where each continuous reaction can occur, integrative of variation
697 in protolith and pressure conditions in thermodynamic models. (b) Occurrences of pyrite (Py),
698 (c) pyrrhotite (Po), and (d) chalcopyrite (Ccp) across metamorphic temperature. Note that
699 samples may host one or all of the identified sulfides.

700

701

Table 1 – Mineral Assemblages and Bulk Compositions for Samples

Unit	Sample#	Rock	Silicate/Oxide Ass	Sulfides	T Gt Bt	TRSCM	SiO2	TiO2	Al2O3	Fe2O3	MnO	MgO	CaO	Na2O	K2O	P2O5	LOI	Total	XMg
PPU	AG006-1	Argillite		py + po + cp		290*													
PPU	AG010	Argillite	chl + mu	po + cp		306*													
LRC	AG029-4	Argillite				323	61.6	0.81	17.3	6.62	0.08	2.72	1.08	2.36	2.74	0.19	4.13	99.7	0.45
LRC	AG140	Phyllite	mu			369													
LRC	AG105-1	Phyllite	mu	py + cp		399*													
LRC	AG056	Phyllite	mu			461*													
LRC	AG101-1	Phyllite	mu			475*	61.5	0.83	17.7	5.71	0.07	2.36	3.01	1.83	2.87	0.16	4.03	100.0	0.45
LRC	AG103-2	Phyllite				485*													
LRC	AG054	Phyllite	bt + qz + mu			498													
LRC	AG135	Phyllite		py		518													
LRC	AG049-1	Spotted Phyl	gt + st + bt	po + cp	596 +/-7	528													
LRC	AG127	Schist	and + gt + st + bt	po		548													
LRC	AG128	Schist	and + gt + st + bt			549													
LRC	AG118	Schist	gt + st + bt + mu			554													
LRC	AG046-3	Schist	gt + st + bt + mu	py + po + cp		561													
LRC	AG042	Schist	and + gt + st + bt	py + po + cp		563													
LRC	AG109	Schist	gt + bt + mu	po		578													
LRC	AG080	Schist	sil + st + gt + bt +	po	597 +/-9	591*	61.2	0.89	18.0	7.73	0.14	3.15	2.27	2.08	2.59	0.22	2.34	100.7	0.45
LRC	AG049	Schist	gt + st + bt	po + cp		596													
PPU	AG089-1	metabasite	chl	py		235	44.4	1.46	20.8	11.13	0.27	3.34	12.57	1.49	0.28	0.20	4.82	100.7	0.37
PPU	AG095-2	metabasite	chl			366	46.9	2.10	12.8	13.16	0.20	7.46	8.86	2.80	0.42	0.28	4.04	99.0	0.53
TCM	AG105-4	metabasite	chl	py + cp		399*	49.3	0.83	18.6	11.57	0.21	4.34	9.34	3.10	< 0.01	0.13	3.32	100.8	0.43
TCM	AG055-1	metabasite	chl + ep + mag			452	49.3	1.43	17.4	10.93	0.17	4.35	7.66	3.45	0.51	0.16	3.09	98.4	0.44
LRC	AG137	Amp Schist	amp + plag + ep + ilm			511	47.0	1.38	17.3	9.68	0.17	8.81	11.42	2.63	0.18	0.12	2.16	100.8	0.64
TCM	AG137	Amphibolite	amp + plag + ep	po + cp		515	48.7	1.13	17.2	9.78	0.26	6.99	12.52	2.17	0.16	0.19	1.00	100.2	0.59
TCM	AG070-2	Amphibolite	amp + ep + qz + cl	po + cp		546	45.6	1.57	15.6	12.49	1.36	6.32	12.56	2.07	0.22	0.25	1.09	99.2	0.50
TCM	AG069-2	Amphibolite	amp + ep + qz + cl	po + cp		548	49.1	1.11	16.0	10.35	0.17	7.61	11.31	2.52	0.13	0.09	2.46	100.8	0.59
TCM	LC 12	metabasite	chl			555	45.8	2.51	19.0	13.09	0.20	4.07	9.39	3.52	0.69	0.39	0.77	99.4	0.38
TCM	AG059	Amphibolite	amp + pl + qz + bt	po		558	61.3	0.75	16.5	6.82	0.23	2.72	2.05	6.20	0.04	0.34	2.59	99.5	0.44
Global**		Pelite					64.1	0.91	19.6	6.85	0.08	2.41	0.65	1.38	3.95				0.41
PPU - Pandora Peak Unit; LRC - Leech River Complex; TRM - Tripp Creek Metabasite																			
amp- amphibole; and- andalusite; bt - biotite; chl- chlorite; ep - epidote; gt- garnet; ilm - ilmenite; mu - muscovite; mag - magnetite; qz - quartz; st- staurolite																			
py - pyrite; po- pyrrhotite; cp- chalcopyrite																			
XMg = molar Mg/(Mg+Fe); TGtBt- T from gt-bt FeMg thermometry (Geen and Canil, 2023)); TRSCM - T from Raman spectroscopy of carbonaceous matter (Geen and Canil, 2023)																			
** Median composition of 5729 world pelites (Forshaw and Pattison, 2023)																			

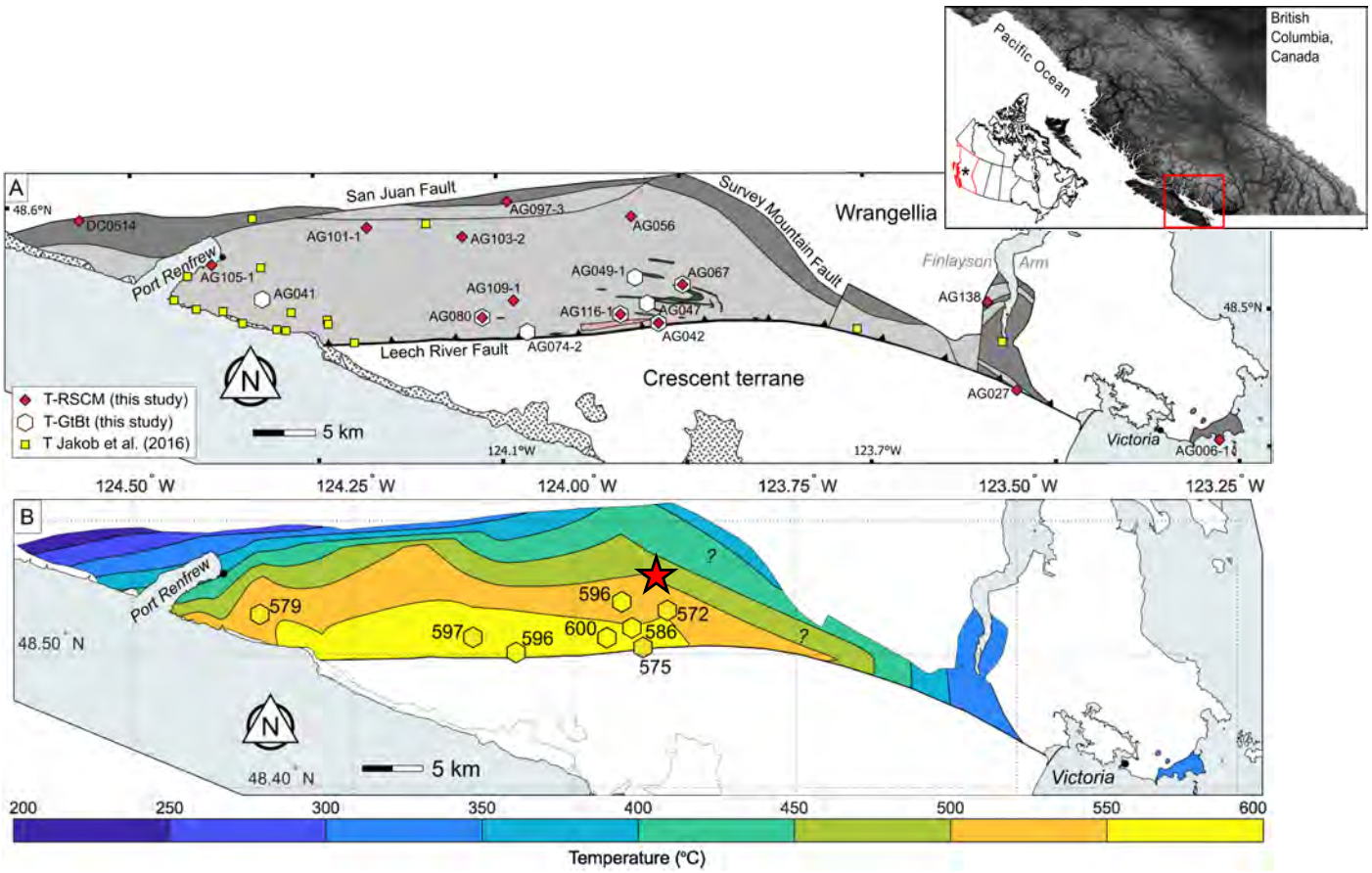
A
48.6°N
DC0514
San Juan Fault
AG097-3
AG101-1
AG103-2
AG056
Survey Mountain Fault
Wrangellia
Finlayson Arm
Port Renfrew
AG105-1
AG041
AG109-1
AG049-1
AG067
AG080
AG116-1
AG047
AG042
AG138
48.5°N
Leech River Fault
AG074-2
Crescent terrane
AG027
Victoria
AG006-1
T-RSCM (this study)
T-GtBt (this study)
T Jakob et al. (2016)
5 km
124.1°W
123.7°W
Pacific Ocean
British Columbia, Canada
124.50° W
124.25° W
124.00° W
123.75° W
123.50° W
123.25° W
B
Port Renfrew
579
596
572
597
596
600
586
575
?
?
48.50° N
48.40° N
5 km
Victoria
200
250
300
350
400
450
500
550
600
Temperature (°C)

Fig 1

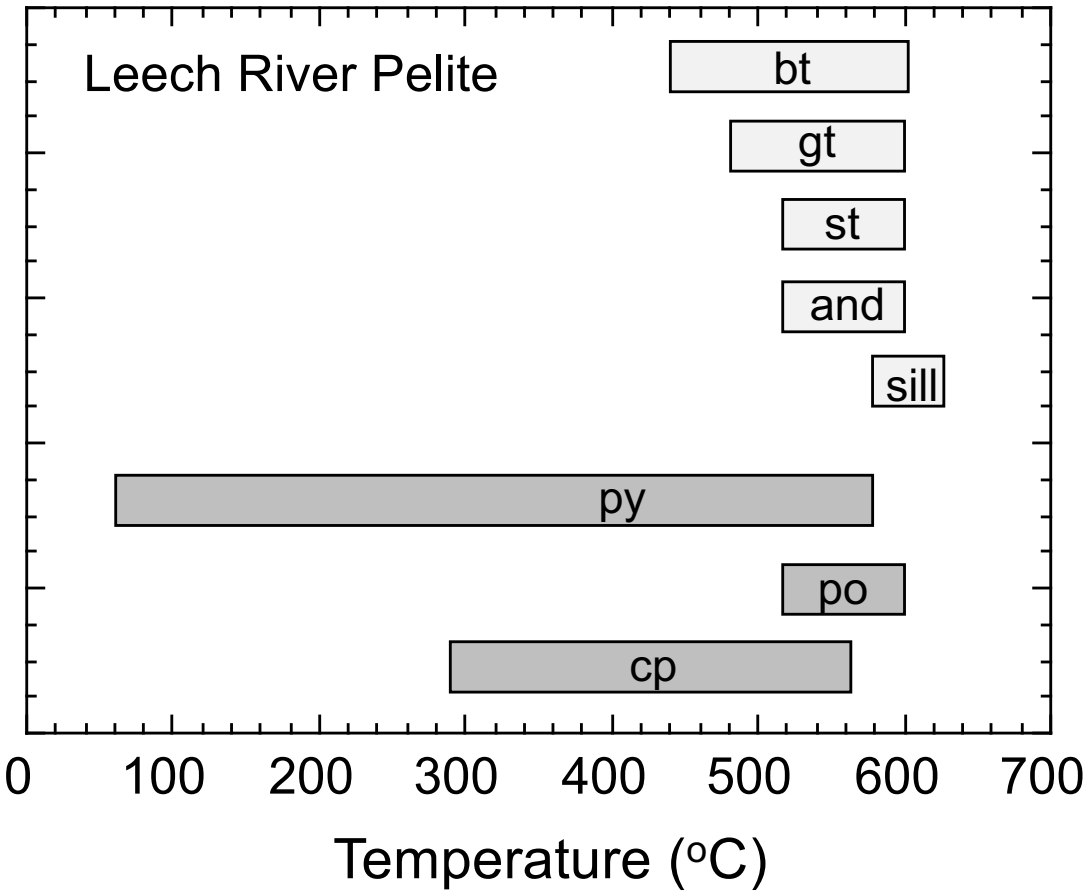
Leech River Pelite
bt
gt
st
and
sill
py
po
cp
0
100
200
300
400
500
600
700
Temperature (°C)

Fig 2

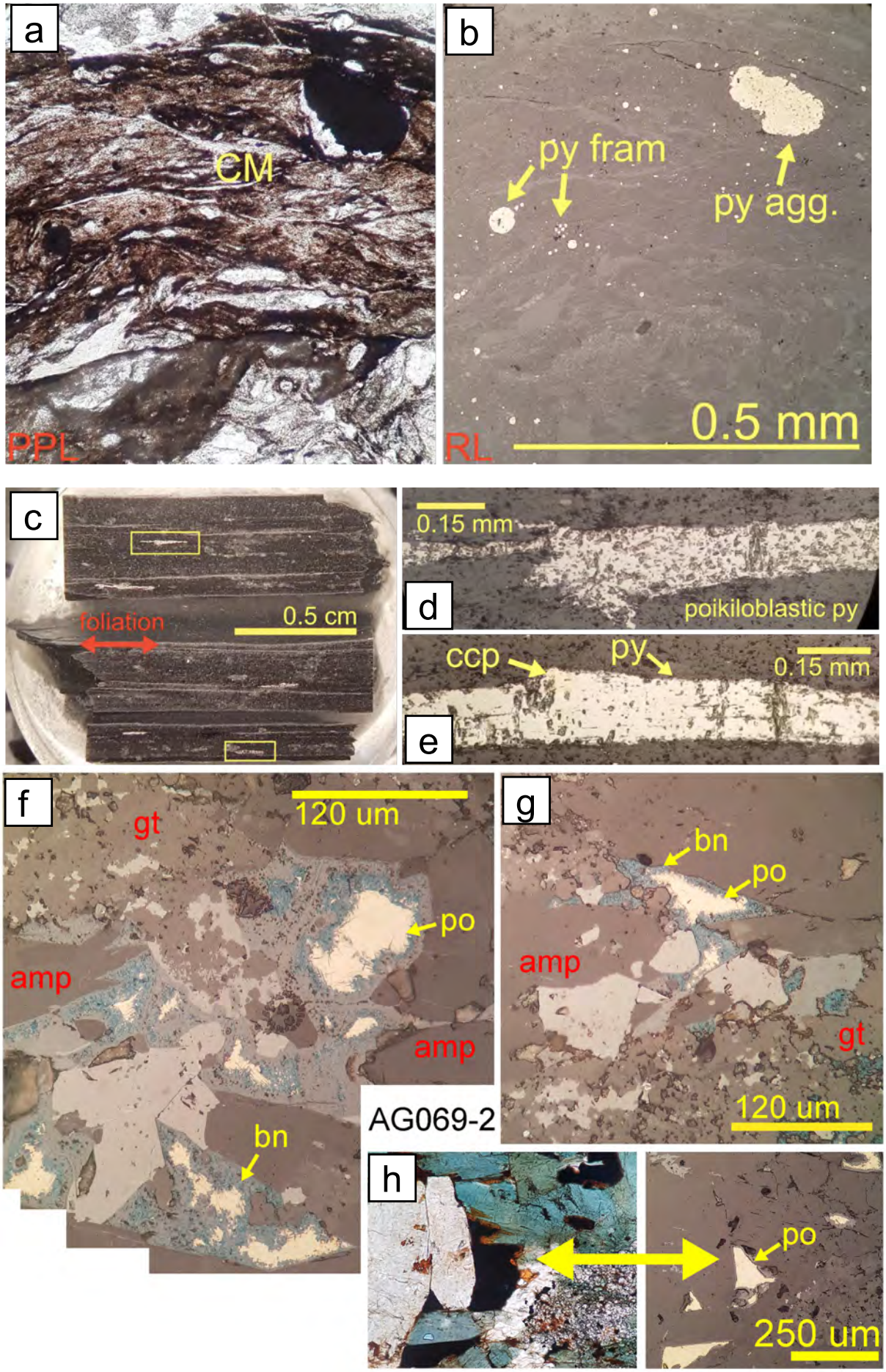
a
CM
PPL
b
py fram
py agg.
RL
0.5 mm
c
foliation
0.5 cm
d
0.15 mm
poikiloblastic py
e
ccp
py
0.15 mm
f
gt
120 um
po
amp
amp
bn
AG069-2
g
bn
po
amp
gt
120 um
h
po
250 um

Fig 3

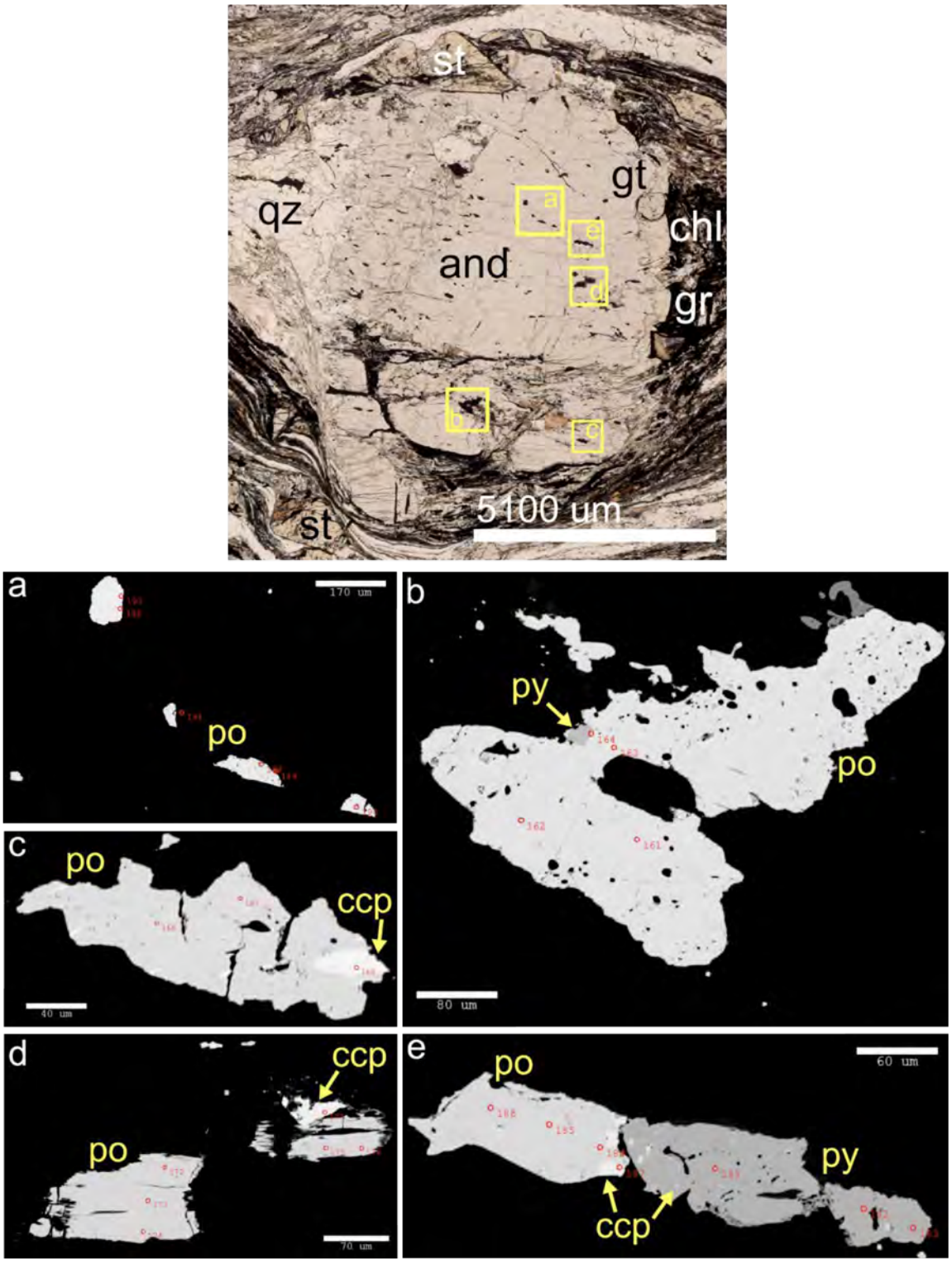
st
gt
qz
chl
and
gr
st
5100 um
a
b
c
d
e
170 um
po
py
po
80 um
c
po
ccp
40 um
d
ccp
po
70 um
e
po
60 um
py
ccp

Fig 4

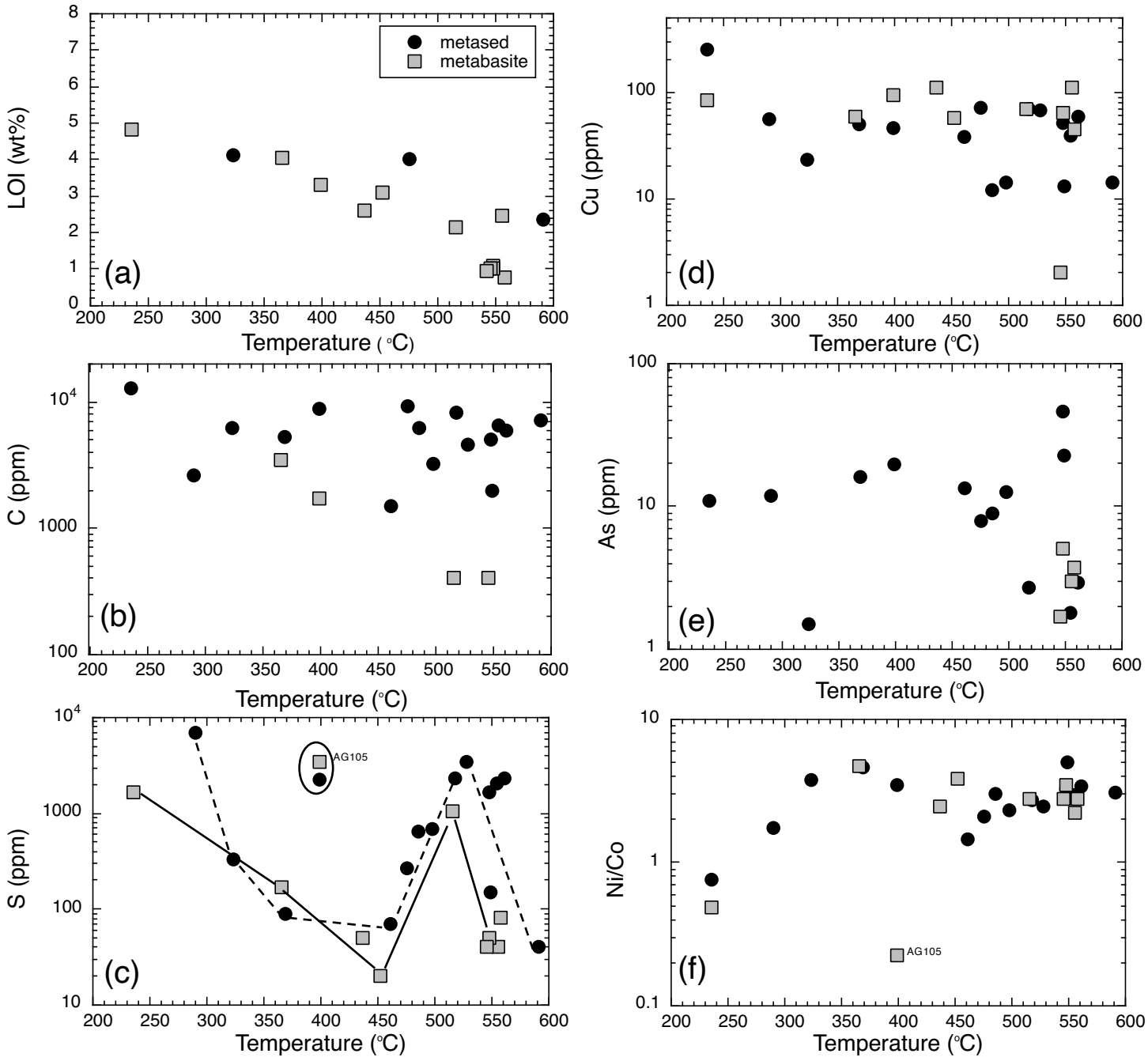
metased
metabasite
(a)
LOI (wt%)
Temperature (°C)
(b)
C (ppm)
Temperature (°C)
(c)
S (ppm)
AG105
Temperature (°C)
(d)
Cu (ppm)
Temperature (°C)
(e)
As (ppm)
Temperature (°C)
(f)
Ni/Co
AG105
Temperature (°C)

Fig 5

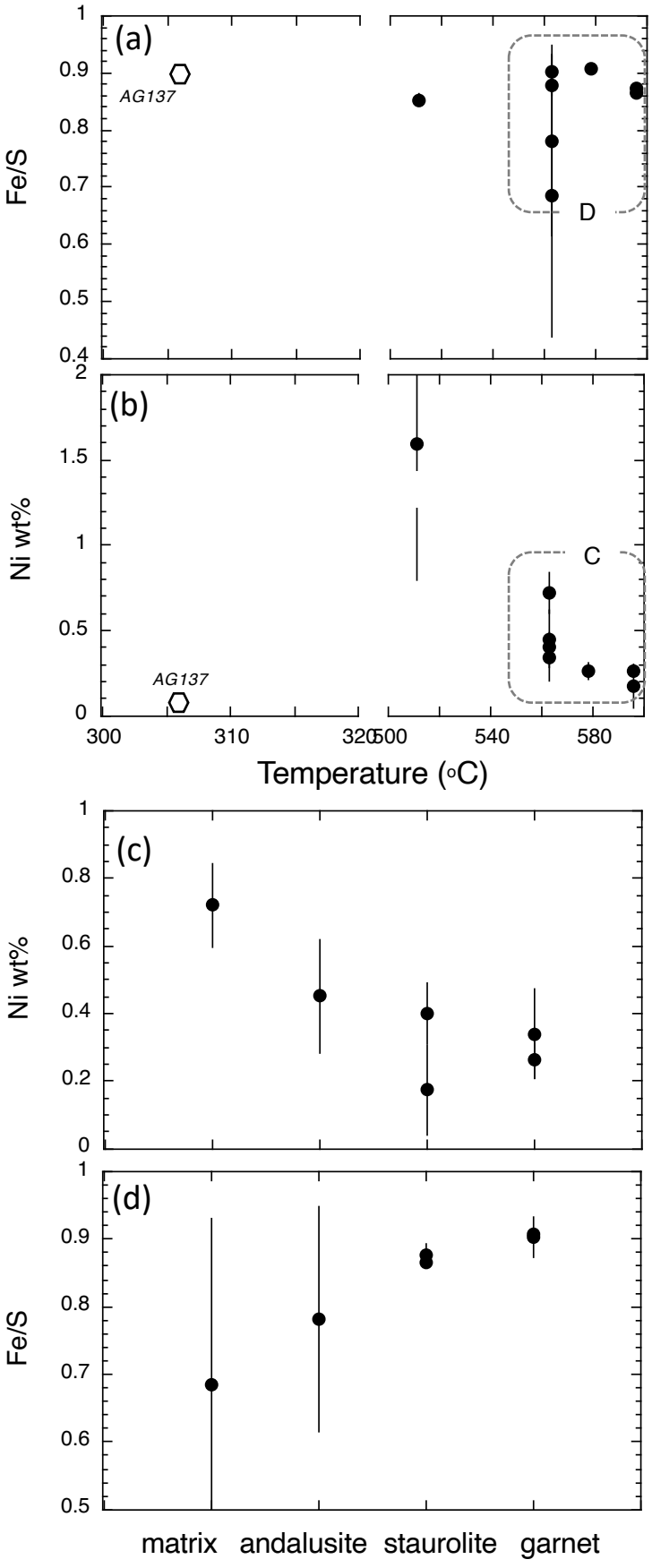
(a)
AG137
D
Fe/S
(b)
C
AG137
Ni wt%
Temperature (◦C)
(c)
Ni wt%
(d)
Fe/S
matrix
andalusite
staurolite
garnet

Fig 6

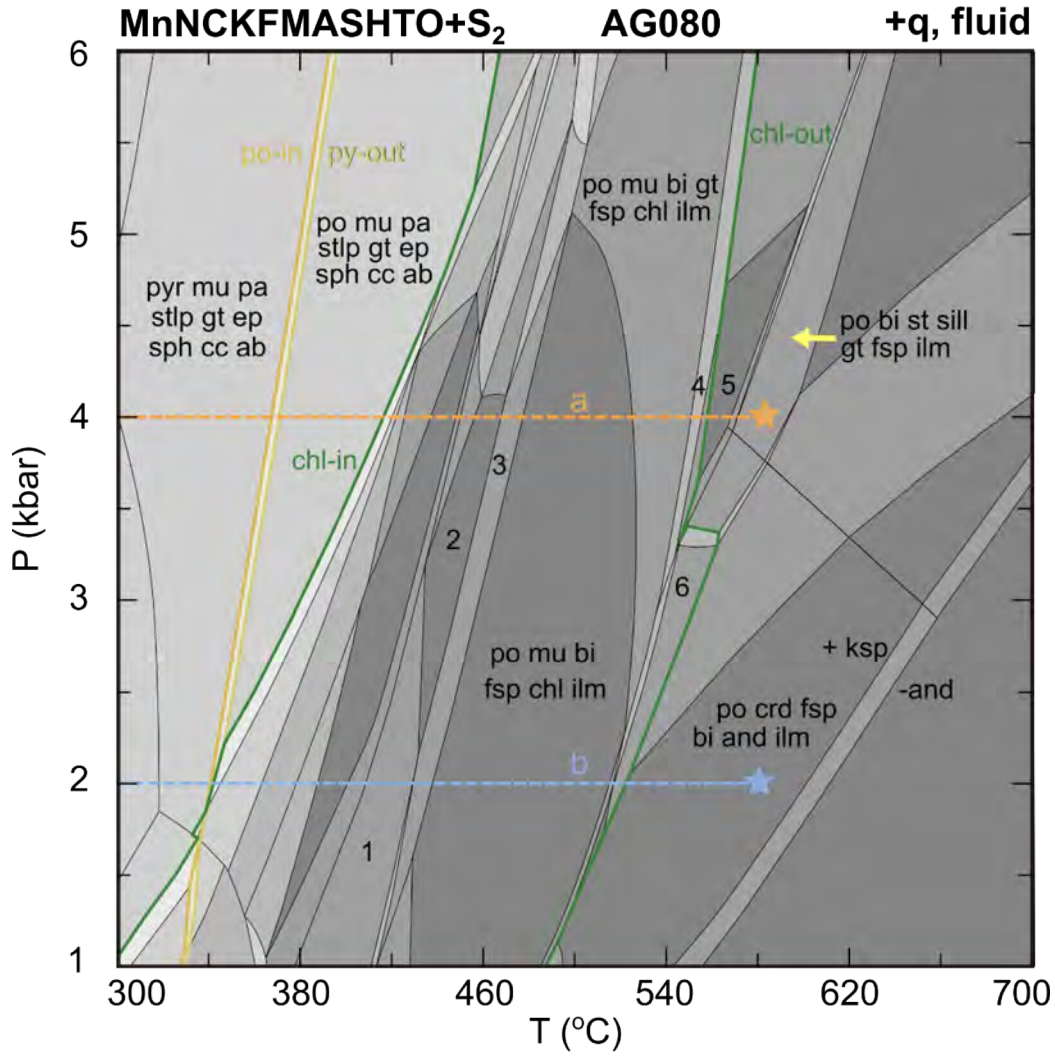

1 - po fsp chl mu bt sph ab	4 - po fsp chl mu bt st gt ilm
2 - po fsp chl bt mu sph	5 - po fsp mu bt st ilm
3 - po fsp chl bt mu sph ilm	6 - po fsp chl bt gt and ilm

Fig 7

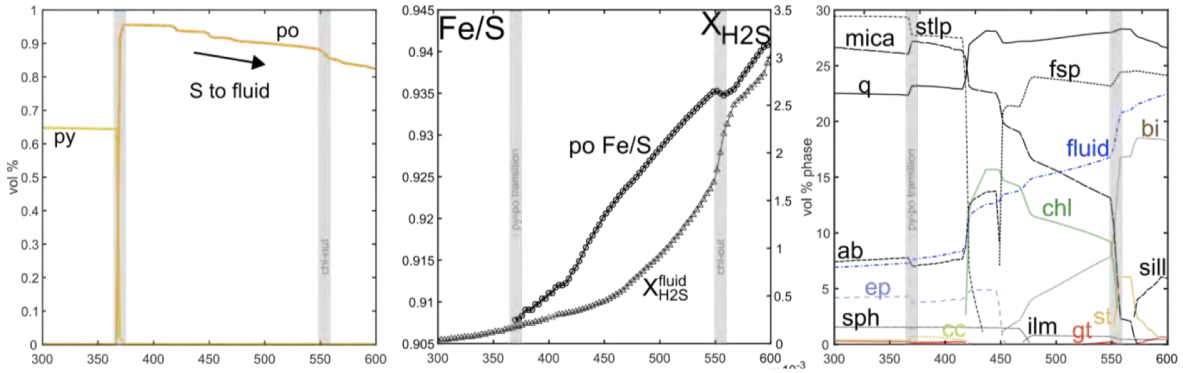
vol %
py
po
S to fluid
py-po transition
chl-out
Fe/S
X_{H2S}
po Fe/S
X^{fluid}_{H2S}
vol % phase
mica
stlp
q
fsp
fluid
bi
chl
ab
ep
sph
cc
ilm
gt
st
sill
Temperature (°C)

Fig 8

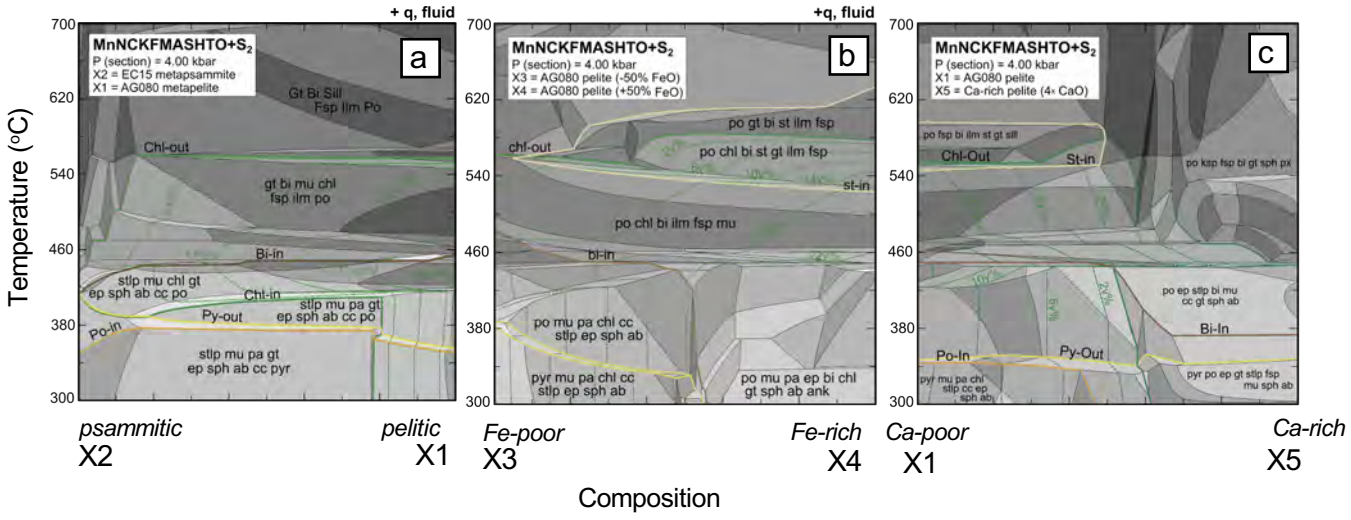
Temperature (°C)
700
620
540
460
380
300
+ q, fluid
MnNCKFMASHTO+S2
P (section) = 4.00 kbar
X2 = EC15 metapsammite
X1 = AG080 metapelite
a
Gt Bi Sill
Fsp Ilm Po
Chl-out
gt bi mu chl
fsp ilm po
Bi-in
stlp mu chl gt
ep sph ab cc po
Chl-in
Py-out
stlp mu pa gt
ep sph ab cc po
Po-in
stlp mu pa gt
ep sph ab cc pyr
+q, fluid
MnNCKFMASHTO+S2
P (section) = 4.00 kbar
X3 = AG080 pelite (-50% FeO)
X4 = AG080 pelite (+50% FeO)
b
po gt bi st ilm fsp
chl-out
po chl bi st gt ilm fsp
st-in
po chl bi ilm fsp mu
bi-in
po mu pa chl cc
stlp ep sph ab
pyr mu pa chl cc
stlp ep sph ab
po mu pa ep bi chl
gt sph ab ank
MnNCKFMASHTO+S2
P (section) = 4.00 kbar
X1 = AG080 pelite
X5 = Ca-rich pelite (4× CaO)
c
Chl-Out
St-in
po ksp fsp bi gt sph px
po ep stlp bi mu
cc gt sph ab
Bi-In
Po-In
Py-Out
pyr po ep gt stlp fsp
mu sph ab
psammitic
X2
pelitic
X1
Fe-poor
X3
Fe-rich
X4
Ca-poor
X1
Ca-rich
X5
Composition

Fig 9

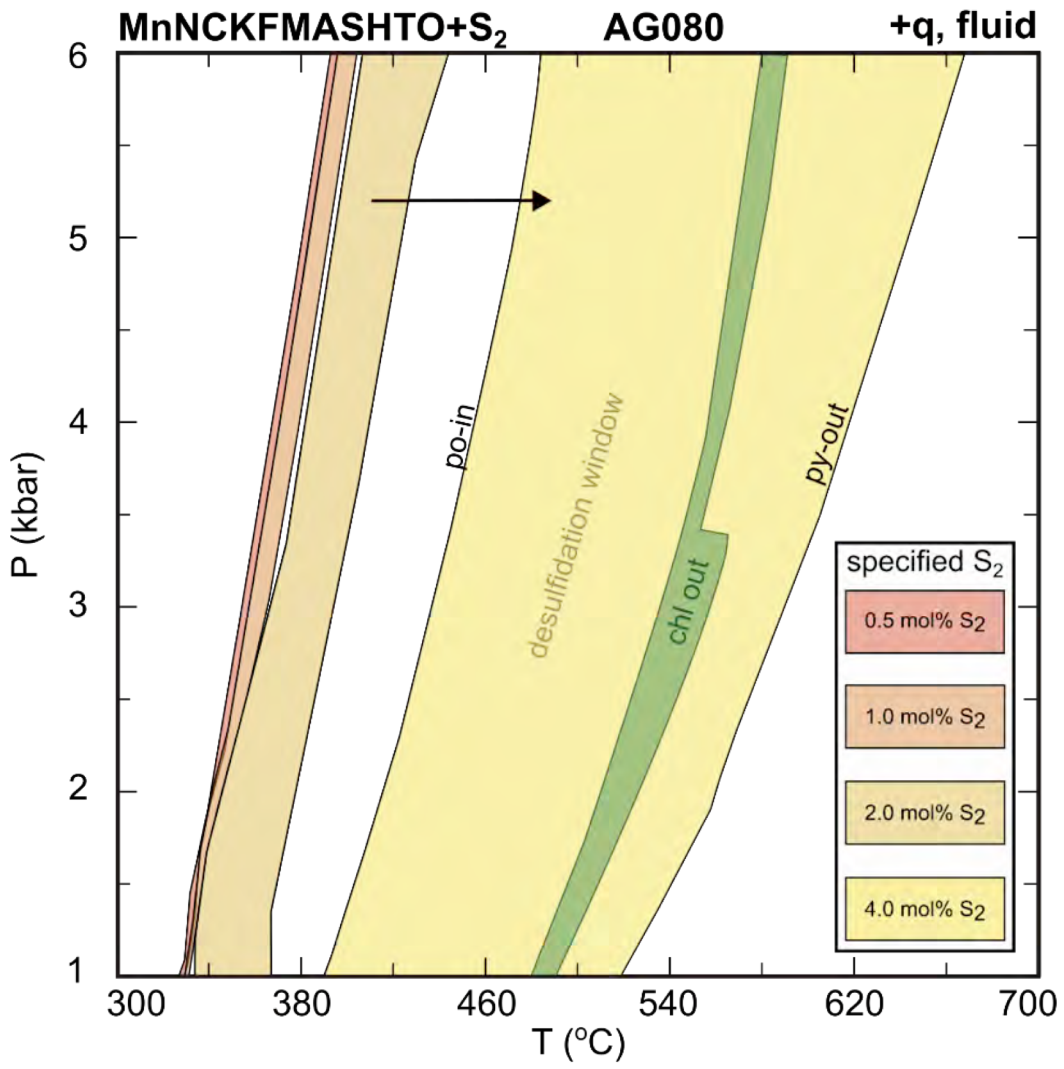
MnNCKFMASHTO+S2
AG080
+q, fluid
P (kbar)
T (°C)
6
5
4
3
2
1
300
380
460
540
620
700
po-in
desulfidation window
chl out
py-out
specified S2
0.5 mol% S2
1.0 mol% S2
2.0 mol% S2
4.0 mol% S2

Fig 10

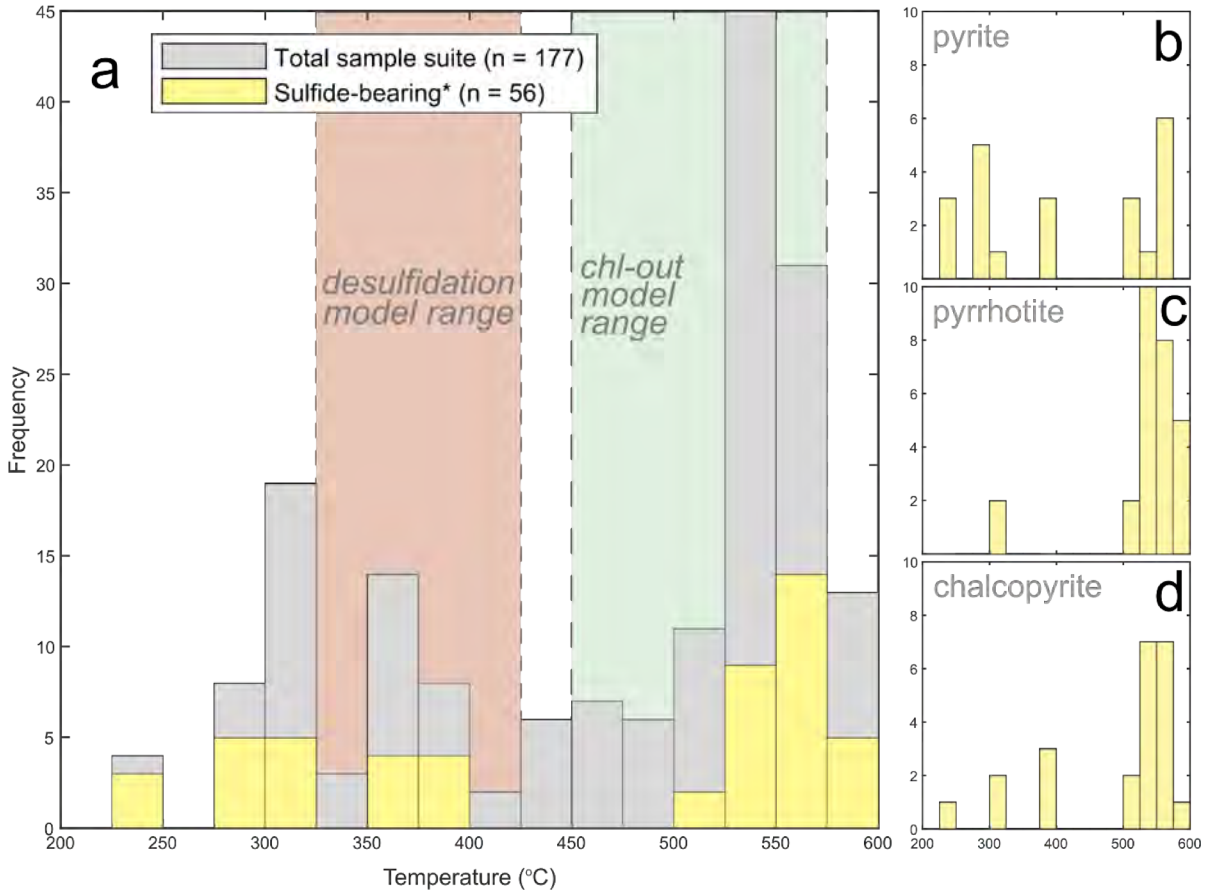
a
Total sample suite (n = 177)
Sulfide-bearing* (n = 56)
desulfidation model range
chl-out model range
Frequency
Temperature (°C)
b
pyrite
c
pyrrhotite
d
chalcopyrite

Fig 11